Journal of Power Sources 260 (2014) 276–291

Contents lists available at ScienceDirect

Journal of Power Sources

journal homepage: www.elsevier.com/locate/jpowsour

On-line adaptive battery impedance parameter and state estimation considering physical principles in reduced order equivalent circuit battery models
Part 1. Requirements, critical review of methods and modeling

Christian Fleischer [a,c,*], Wladislaw Waag [a,c], Hans-Martin Heyn [a,c], Dirk Uwe Sauer [a,b,c]

[a] Electrochemical Energy Conversion and Storage Systems Group, Institute for Power Electronics and Electrical Drives (ISEA), RWTH Aachen University, Jägerstrasse 17/19, 52066 Aachen, Germany
[b] Institute for Power Generation and Storage Systems (PGS), E.ON ERC, RWTH Aachen University, Germany
[c] Jülich Aachen Research Alliance, JARA-Energy, Germany

HIGHLIGHTS

- Definition of BMS requirements for low-cost microcontroller.
- Critical review on commonly used methods, elaborating on strengths and weaknesses.
- Battery model considering Butler–Volmer kinetics on the charge-transfer process.
- Mass transport process inside the battery is modeled in a novel state-space equation.

ARTICLE INFO

Article history:
Received 8 November 2013
Received in revised form
7 January 2014
Accepted 23 January 2014
Available online 5 March 2014

Keywords:
Battery monitoring
Parameter & state estimation
Impedance
On-line recursive algorithm

ABSTRACT

Lithium-ion battery systems employed in high power demanding systems such as electric vehicles require a sophisticated monitoring system to ensure safe and reliable operation. Three major states of the battery are of special interest and need to be constantly monitored, these include: battery state of charge (SoC), battery state of health (capcity fade determination, SoH), and state of function (power fade determination, SoF).

In a series of two papers, we propose a system of algorithms based on a weighted recursive least quadratic squares parameter estimator, that is able to determine the battery impedance and diffusion parameters for accurate state estimation. The functionality was proven on different battery chemistries with different aging conditions.

The first paper investigates the general requirements on BMS for HEV/EV applications. In parallel, the commonly used methods for battery monitoring are reviewed to elaborate their strength and weaknesses in terms of the identified requirements for on-line applications. Special emphasis will be placed on real-time capability and memory optimized code for cost-sensitive industrial or automotive applications in which low-cost microcontrollers must be used. Therefore, a battery model is presented which includes the influence of the Butler–Volmer kinetics on the charge-transfer process. Lastly, the mass transport process inside the battery is modeled in a novel state-space representation.

1. Introduction

Battery systems are conquering more and more applications. Modern bikes with assisting electrical drive, hybrid or full electric vehicles and even modern aircrafts require battery systems with new dimensions of power capability and energy density. Mobile applications such as electric vehicles rely on the possibility to store energy. Lithium-ion batteries, for example, allow the storage of

* Corresponding author. Electrochemical Energy Conversion and Storage Systems Group, Institute for Power Electronics and Electrical Drives (ISEA), RWTH Aachen University, Jägerstrasse 17/19, 52066 Aachen, Germany. Tel.: +49 241 80 97158; fax: +49 241 80 92203.
E-mail address: cfl@isea.rwth-aachen.de (C. Fleischer).

http://dx.doi.org/10.1016/j.jpowsour.2014.01.129
0378-7753/

energy with an incredibly high coulombic efficiency of nearly 100% [1]. Furthermore, the falling prices for modern battery systems make it more likely that applications with huge energy storages such as full electric vehicles will conquer the mass-markets in the near future.

The downside of modern battery systems are the complex physical processes occurring inside the battery during operation. Sophisticated monitoring systems are necessary to ensure safe and economical operation of the battery systems. Three major states of the battery are of special interest and need to be constantly monitored. First, one needs to know how much energy is currently stored inside the battery, the state of charge (SoC). Second, it is necessary to know the battery system's state of health (SoH). Aged batteries can cause unexpected system failures, thus, foreseeing upcoming failures of the battery system is a major task of battery monitoring systems. Failure of foreseeing a battery fault can cause extreme situations, such as, for example, the lithium-ion battery system of Boeing's new Dreamliner aircraft which caused a fire in the cockpit, resulting in an unacceptable situation in an aircraft [2]. Furthermore, it is necessary to know how much power can be withdrawn from the battery. The third major state of interest, the state of function (SoF), is required to evaluate the battery's power capability for a given operation condition at a given moment, which is necessary to know how much power can be withdrawn from the battery. In conventional vehicles, also with stop/start function, the state of function is mainly determined by the cranking capability of the battery. However, the power capability of the battery in an electric vehicle needs to be known at every moment of operation. A battery failing to deliver the necessary power during a power consuming maneuver such as, overtaking on the highway, is unacceptable.

Resulting from all the aforementioned downsides of modern battery systems, the first paper discusses the requirements on BMS specifications for HEV/EV environment, followed by a critical review on commonly used methods, elaborating on their strengths and weaknesses in terms of the identified requirements for on-line applications. The remainder of this paper employs a battery model to help understand the underlying physical and chemical principles with variable parameters, including the influence of the Butler–Volmer kinetics on the charge-transfer process. Furthermore, the mass transport process inside the battery is modeled in a novel state-space representation.

The second paper presents a novel approach to determine the beforehand mentioned state of charge, state of health and state of function of batteries that are used inside high power and high energy demanding applications such as an electric vehicle. For this purpose, a multi-stage online parameter identification technique is used to determine the parameters of the proposed battery model during operation of the battery. A novel mutation-based algorithm is developed to determine the nonlinear current dependency of the charge-transfer resistance as well as diffusion. The identified parameters are verified on several batteries and at different operation and aging conditions. The algorithm guarantees a short response time and, together with its fully recursive structure, assures a long-term stable monitoring of the battery parameters. The relative dynamic voltage prediction error of the algorithm is reduced to 2%. The changes of parameters are used to determine the states of the battery. The proposed techniques reduce the inaccuracy of State-of-Charge (SoC) estimation to less than 3%. The algorithm is real-time capable and can be implemented on embedded systems. Because it is a fully adaptive approach with an extremely fast response time, it does not require any kind of parameterization nor cell testing. The two paper series is organized as illustrated in Fig. 1.

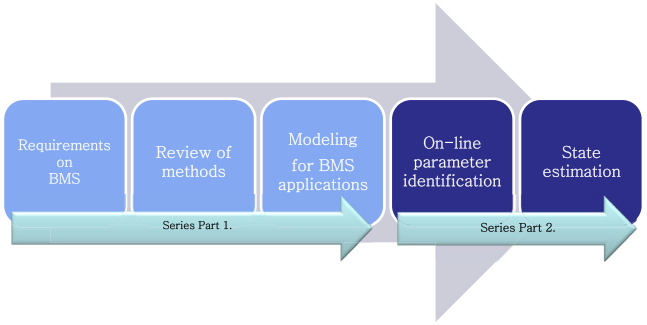

Fig. 1. Organization of the paper.

2. Requirements on battery monitoring algorithms

In most applications, a single cell battery does not generate enough power to fulfill the requirements. Therefore, identical cells are connected together to form large packs. At this point, battery management systems (BMS) are used. The main task of a BMS is to use the battery pack so that it can provide a sustainably high performance and a high amount of energy. It is to maximize the life and ensure a safe operating point. Especially with the use of lithium batteries, close monitoring is necessary and the specified operating limits must be strictly adhered to. Thereby, the BMS takes on a variety of tasks, most importantly:

- Cell monitoring
- Energy management during charging and discharging
- Temperature management
- Cell balancing
- Determination of required parameters and states: SoC; SoH, SoF (available charging and discharging power), battery impedance parameters estimation, capacity, residual energy, remaining useful life (RUL), charging time;

Cell monitoring involves measuring the voltage and temperature of individual battery cells, which must never leave the specified safe operating area (SOA):

- minimal and maximal voltages for each individual cell (predefined by the manufacturer)
- maximum temperature (predefined by the manufacturer)
- maximum discharge current and maximum charge current (dependent on battery condition)

These limits, which must be respected in battery monitoring algorithms depend on the battery conditions or the manufacturer's specifications. Besides the measurements hardware for data acquisition with standard functions, the real key function of the BMS are the corresponding algorithms, that provide the necessary information about the battery states. Therefore, the internal and external battery characteristics, referring to the battery's current and voltage, for different conditions and parameters such as temperature, present battery load, SoC, history, impedance parameters or capacity have to be considered. It is of particular interest to identify the change of described characteristics through battery aging. To simplify the monitoring system, independent conditions can be excluded beforehand. The specified limits are the limiting factor of the available battery energy and power, which depend on current conditions. For example, conventional BMS prohibit or reduce charging power to a minimum at low temperatures to prevent lithium plating. Also, further restrictions or stricter limits

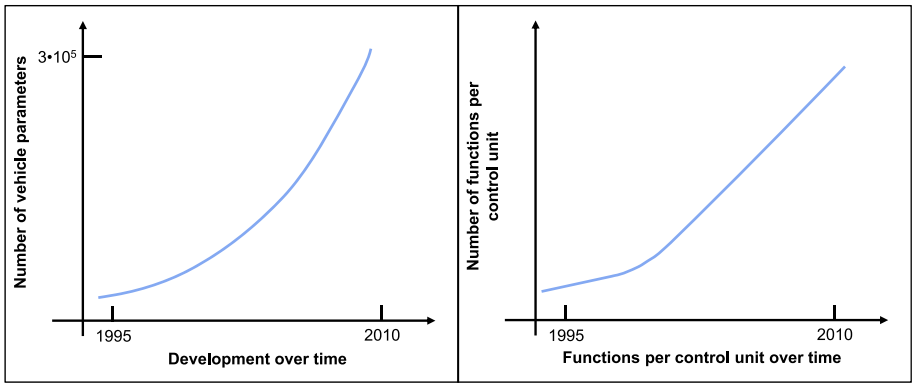

Fig. 2. Development of performance requirements for ECUs in automotive industry [3].

(e.g. SoC operating range) besides the manufacturer's SOA prevent excessive aging. A further important point, which is often ignored, discusses the characteristics of the target platform consisting of measurement electronics and master controller executing monitoring algorithms. The most relevant measurements are the voltages of every cell of the battery pack, the current flowing through each battery pack in parallel, and the temperature of each battery cell or at least of some points within the battery pack that are thermally critical. The measurements for voltage and current must be sampled fast enough to catch all relevant dynamics. The limitation of the voltage and current low-cost measurement has to be considered. While the accuracy of the voltage measurement can be measured in a range between 10 mV and 30 mV, the measurement of an accurate battery current in low-cost applications is certainly a challenging task. Mainly the current shunt or hall sensor is used. However, current shunts are not isolated from the battery pack which might pose a safety risk; furthermore their precision is influenced by temperature and the shunt consumes some energy. Hall sensors are more expensive to implement and they suffer from an offset that has to be re-calibrated regularly.

In addition, and this is important, while the application parameters and functions in vehicles shows exponential growth in Fig. 2, at the same time the amount of controllers with computing power and memory show only limiting growth (Fig. 3). Generally speaking, this means that requirements on memory optimized code have become more demanding.

For cost reasons e.g. integrated floating point unit (FPU) is skipped, making fast calculations and evaluations of complex mathematical algorithms impossible. Therefore, the demands being made of the on-line monitoring software are growing and diverse; for example, in the developing process, it must be ensured that models can be converted into fixed-point arithmetic requiring less computer processing power compared to FPU emulation [4]. Many requirements, decisions and operations as summarized in Table 1 need to be taken into consideration to ensure for the road safety of the passengers and vehicle. The BMS must have real-time capable control to keep up with the physical processes. Therefore the demands on safety, performance, and reliability of such software are very high. It will be necessary to ensure that it is a traceable and high-quality software for analyzing and remedying complex system errors. In order to ensure this, algorithms have defined mathematical model functions with clear and unambiguous description based on physical or electro-chemical relations. Attention must also be paid to the systems scalability to different applications and battery technology. The modular development of model-based design also provides an adequate flexibility, for example when switching to $LiFePO_4$ cells leading to the necessity of adjusting the hysteresis model.

Lastly, the influences of history and current battery load profiles have to be considered for battery monitoring. As shown in Ref. [5] high dynamic load profiles lead to different estimated impedance parameters leading, for example, to different temperature

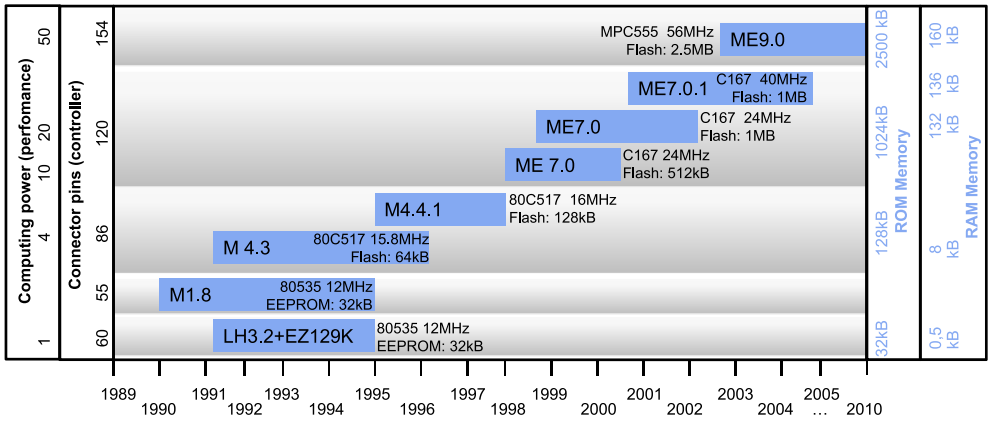

Fig. 3. Development of control units in automotive industry [3].

Table 1
Important requirements for the BMS software in automotive industry [3].

Requirements	Examples of fundamental requirements
Functional requirements	Real-time capability through high-speed compute cycles; transmission of large volumes of data; scalability for modular battery system (series/parallel configuration, from light to heavy duty commercial vehicles); adaptability to different chemistries
Diagnostic requirements	Monitoring of safety-related functions; diagnostic capability at service station; monitoring of the relevant driving safety functions;
Economic requirements	Maintainability, re-usability due to adaptation; memory optimized code; modular design; long lifecycle;
Organizational requirements	Development across distributed locations;

distribution within the battery pack in comparison to passive battery load profiles.

3. Review on commonly used methods for battery monitoring

Monitoring algorithms have to be able to modify their parameterization to the battery changing condition to be able to estimate exact states during battery lifetime. Many different approaches for monitoring lithium-ion batteries in battery electric vehicle (BEV) and hybrid electric vehicle (HEV) are discussed in the literature. Fig. 4 summarizes the commonly used methods in parameter and state estimation, which will be discussed in the following and more in detail in Refs. [4,6]. The parameter estimation methods can be divided into three subgroups, first the methods using impedance spectroscopy (EIS) which is normally carried out in the laboratory using complex measurement equipment. Based on this some researcher use active signal generator in the field. However, these methods need in addition special electronics. To keep the costs low, passive impedance spectroscopy [7,8] was introduced for lead-acid and applied to lithium-ion batteries. The difference between the two methods is that the passive system utilizes the fluctuations of current triggered by battery load. The main challenge therefore, consists of systematic incidences of the frequency range to calculate the impedance. Moreover, through the usage of linear filters, important information e.g. which is needed to calculate the Butler–Volmer equation, will get lost. The second subgroup from parameter estimation methods is based on traditional lithium-ion battery equivalent circuit models. Based on the dynamic characteristics and working principles of lithium-ion batteries, equivalent circuit models are used consisting of resistors, capacitors and voltage sources forming a circuit network to describe battery dynamics. To identify the unknown model parameters and states, dual (DKF) or joint Kalman filters (JKF) may be used. The DKF consists of two different Kalman filter in which the results are calculated in parallel and results of the respective is feed to its counterpart. It is therefore possible that states and parameters are calculated separately. In JKF states and parameters are re-adapted at the same time increasing computing effort due to higher model matrices. However, still JKF increases estimation accuracy [9–16]. The applied filter are, e.g. in Refs. [9,17–19] the dual extended Kalman filter (DEKF) is applied, in Refs. [20,21] the joint extended Kalman filter, in Refs. [12,22] the dual sigma-point Kalman filter (DSPKF), in Ref. [23] the joint sigma-point Kalman filter (JSPKF) and in Ref. [24] the particle filter (PF). These methods require high computing power, may lead to numeric instability, in most cases assume Gaussian noises and lack in the approximation of the non-linear system especially during high battery dynamics [4]. Often the more standard and classic approach of *least squares* (LS) is applied to estimate the best solution of an overdetermined system to minimize the sum of squared residuals. The employed variations of LS are the recursive least squares filter (RLS), the recursive least mean square (LMS) filter and the weighted recursive least squares filter (WRLS) and applied in Refs. [25–32]. The general advantage to the earlier Kalman filter variations is the lower computational cost due to required matrix inversions for KF, and also, LS do not need to store significant amount of data. However, when one looks at the literature about the development of monitoring algorithms, the approaches lack on temperature and accurate current dependency of the battery charge transfer resistance and require higher degree of battery models to prevent divergence problems. Nevertheless, WRLS techniques provide additional expansion opportunities.

On the other side, non-recursive filter are using batch learning by storing the measured battery current and voltage temporarily in the RAM, in the following the iterative least squares procedure is deployed to fit the battery model to the measured data [33,34]. This enables to estimate parameters of a highly non-linear system without lacking rigidity. Then again, it demands memory and computing power for the parameter search, the high frequency real-time parameters might change during evaluation and therefore are not up-to-date in the corresponding operating point. In Refs. [35–37] electro-chemical models in combination with linear and sigma-point Kalman filter are used to estimate the internal battery potentials, electrolyte conductivity and SoC to draw conclusions on the internal resistance. In Refs. [37–44] partial differential equations (PDE) and single particle models are combined with back-stepping observers, Padé-based approximations and LS principles to allow dual state (SoC) and parameter (internal resistance) estimation. Unfortunately the literature is missing to debate on the applicability of electro-chemical models for on-line monitoring operation. The immense amount of complex calculations not only of the models but also the adaptive filters puts a question mark at the usage on low-cost microcontrollers. Even though parameter estimation is a great and important task of battery monitoring, in some applications the state estimation is the only actual function. Thereby, SoC estimation is integrated as a basic feature. Many different approaches are discussed in the literature, however, when the current measurement electronics are precise and the battery capacity is known, ampere hour balancing (AHB) is a very accurate and low-cost method for lithium-ion batteries. Nevertheless, the provisions of initial SoC knowledge and re-calibration after long-term (possible accumulated measurement errors) operation must be met. Often, the open-circuit-voltage (OCV)–SoC relation is utilized for SoC estimation. For lithium-ion batteries with lithium nickel cobalt oxide ($Li(Ni,Co)O_2$, NCA) or nickel manganese cobalt oxide (LiNiMnCo, NMC) cathodes the OCV–SoC relation has a very distinct characteristic. This relation has a minor change over the battery lifetime [5], however, batteries with lithium iron phosphate ($LiFePO_4$, LFP) cathode require a hysteresis model [45–49]. These models are complex and often a source for errors. For e.g. Refs. [50,51] estimating battery electromotive force (EMF), the equilibrium battery voltage at the end of OCV process is used instead. It uses an empirical equation to estimate the EMF. To account for the aging, in Ref. [51] an adaptive method for a voltage relaxation model described by an exponential function is used. Both methods approximate the relaxation process relatively inaccurately. In Ref. [52] the authors improve the empirical model which leads to better results. The model based SoC estimation employs adaptive filters and observes such as various Kalman, Gauss–Hermite quadrature, H-infinity and particle filters. First the ordinary linear Kalman filter was applied until additional key steps were developed, such as extended Kalman filter (EKF) and the principles of Monte Carlo analysis. From then on it was possible to use higher order complex and non-linear battery models. In Refs. [53–56] different battery models with EKF were applied. The drawback of EKF is that it

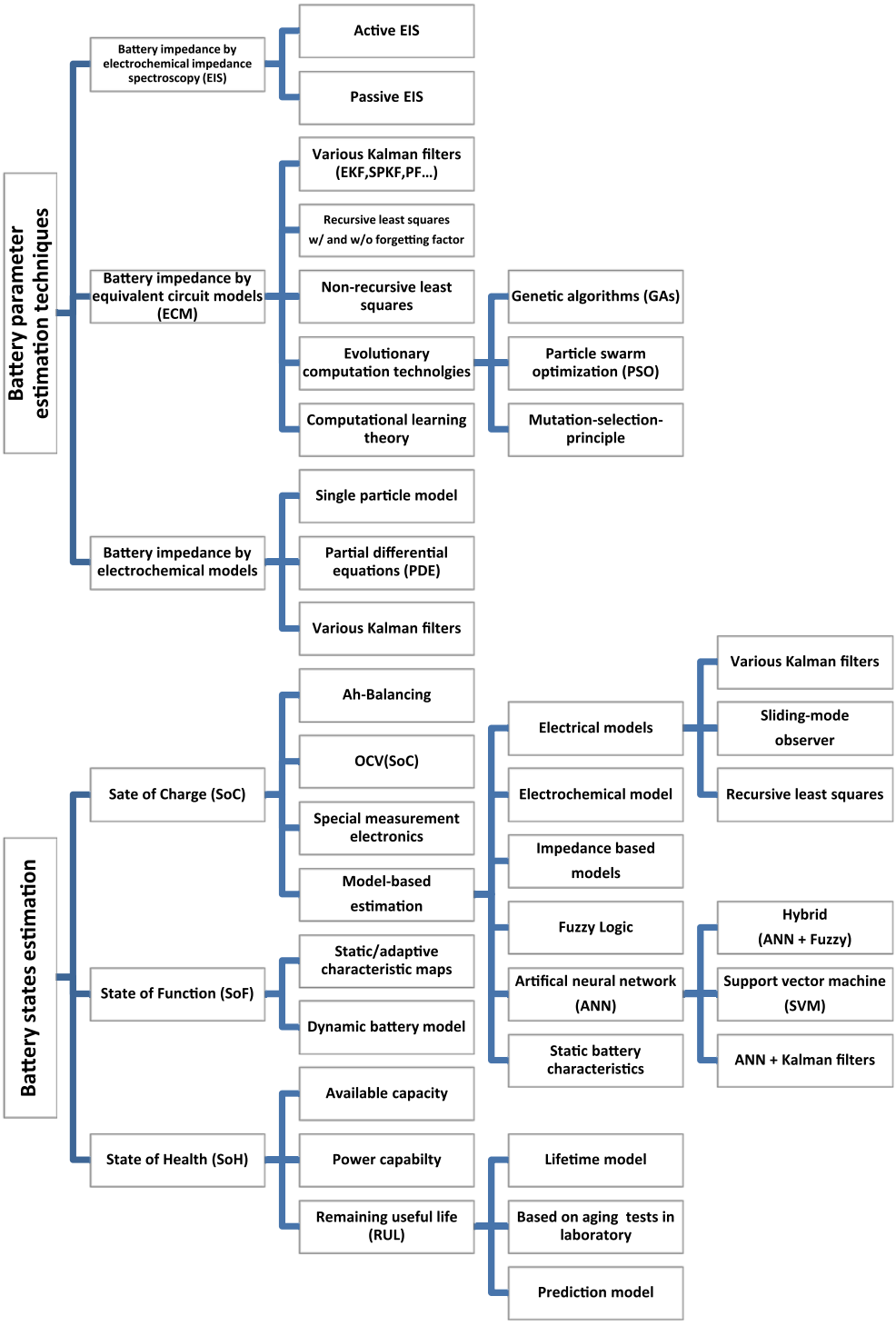

Fig. 4. Commonly used methods for battery monitoring in scientific publications.

linearizes the non-linearity in the battery model about an estimate of the current mean and covariance which may lead to inaccurate estimates especially for high dynamic load profiles. It is also assumed that process and observation noises are zero mean multivariate Gaussian noises, which may differ in the field. The unscented transformation (UT) was suggested by Julier and Uhlmann in Refs. [57–59] using the exact nonlinear function which is applied to the approximating probability distribution function (PDF). The original SPKF (UT-based unscented Kalman filter (UKF)) was first formulated in its extended form in Ref. [60] and applied for SoC estimation in Refs. [61–63]. Most of these implementations are prohibited for on-board implementation due to their overload in computational complexity. Advanced marginal filtering principles such as central difference Kalman filter (CDKF) [11], scaled unscented transform Kalman filter (SUKF) or spherical simplex unscented Kalman filter (SSUKF) [64] require less calculating power. Gauss–Hermite quadrature filter (GHQF) is an alternative to SPKF with similar structure but differ in generation of sigma points and

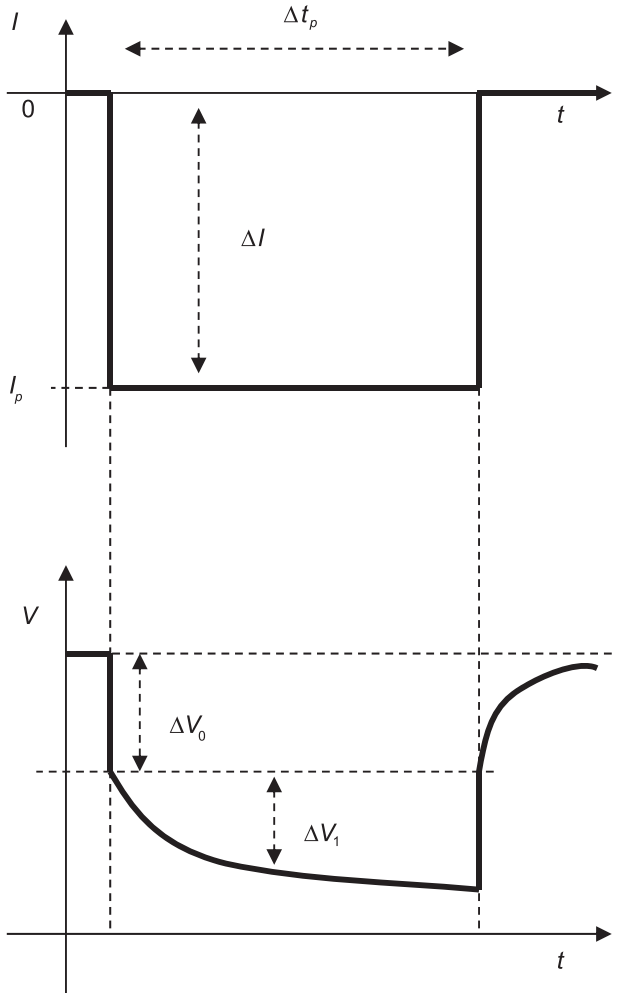

Fig. 5. Applied current pulse to the battery and its voltage response for DCR extraction [4].

weights. Additionally, adaptive filter such as adaptive extended Kalman filter (AEKF) [65] or adaptive sigma-point Kalman filter (ASPKF) are used for adaptive adjustment of the noise covariances [66]. For applications where model and measurement uncertainties are unknown, H-infinity (H_∞) filter may be used [67]. Sequential Monte Carlo (SMC) methods (particle filter (PF)) using directly the Bayesian recursion equations to estimate the posterior density function. Similar to the UKF it transforms a set of points, however, in PF the points are chosen randomly and the amount needs to be much higher. The PF may result in better results at the cost of additional computational effort [68]. These filters depend on the underlying battery model, and in some situations lacks observability, e.g. during constant current phase. The parameterization of the battery models needs to be carried out in the laboratory and online parameter estimation has to adapt the model parameters to the current aging state (e.g. joint/dual KF) which increases the demand on computing power. A number of state observers such as sliding mode observers [69], adaptive Luenberger observer [69] for SoC estimation are discussed in the literature. For these methods additional algorithm for battery model parameter estimation is needed. RLS filter for SoC estimation may be used as an alternative to KF. They can be more efficiently implemented on low-power microcontroller due to less computational effort. On the other hand, divergence problems may lead to instability. Instead of using electrical models for SoC estimation, electro-chemical models are used [70] in combination with KF. These models take battery behavior into consideration without the need for storing parameters into characteristic maps. The combination of complex models and adaptive filter exceeds the applicability on automotive controller. Impedance-based SoC estimation [71] lacks on accuracy while aging proceeds. Exact information regarding temperature is crucial due to stronger parameter dependencies on temperature than on SoC. Occasionally, methods of machine learning (fuzzy logic, artificial neural networks (ANN), support vector machines (SVM) and hybrid systems such as adaptive neuro fuzzy inference systems (ANFIS) are developed. In fuzzy logic systems the battery SoC is inter-connected with the measured battery current, temperature and voltage and is therefore rather static. ANN SoC estimation focuses mainly on the voltage prediction in combination with KF [72], combination with AHB or direct method. ANN does not use mathematical models to describe battery dynamics, moreover the network is trained with collected testing data. For the direct approach, the open-loop principle makes it impossible to adapt to the aging state of the battery. To overcome this backwardness, various KF may be applied where the estimated output voltage is compared to the measured battery terminal voltage and used for SoC correction [73]. Fuzzy inference systems and neural networks are well-known methods for modeling nonlinear systems. Both approaches have strengths, but also drawbacks. Fuzzy inference systems can "fuzzily" incorporate human knowledge in modeling in the kind of if–else statements, but they are not able to capture measurement samples and use them to adjust system parameters. However, neural networks possess the capability of learning by the use of measurement samples in order to adapt the input–output mapping to changing conditions. The SoC estimation of the hybrid system is discussed in Refs. [74,75]. However, to consider battery aging, complex learning algorithms are necessary. Also, a problem will occur, if not the whole input space (universe of discourse) of one input variable is properly trained, but only a small region resulting ANFIS to be overfitted in a certain region. A further key element in state estimation is the SoH. SoH estimation can be subdivided into capacity and impedance estimation. The discussed methods in the literature for capacity estimation can be summarized into three groups. Group one evaluates the measured OCV right before charging e.g. after discharging [76,77]. Only the relation SoC-OCV as parameter is needed, however, for BEV the OCV condition for low SoC might not be fulfilled due to immediately charging process. The second group focuses on the estimation of the OCV change under load e.g. Ref. [78], makes it independent from OCV condition. However, exact battery parameters, such as internal resistance must be known. Finally, the third group utilizes an electrical battery model in combination with adaptive filter integrated in the state equation [15,23,79]. A different approach is based on incremental capacity analysis (ICA) and differential voltage analysis (DVA) techniques. Here, the gradual changes in electro-chemical properties are determined by linking the charge–voltage curves onto dQ/dV peaks with different amplitudes. These characteristic peaks change in time and amplitude [80]. However, this method requires constant current charging and discharging phases which is virtually non-existent in PHEV/EV applications. An aspect that is increasingly important within battery monitoring systems is the SoF estimation, here we define it as the state of available power (SoAP). Conventional state of the art methods for SoAP prediction can be categorized into two groups: 1.) based on battery characteristic maps and 2.) equivalent circuit models to describe the battery dynamics. For the first group, extensive cell tests are carried out in advance to generate a dependency between the available power of the battery in regard to the battery states (eg. SoC, temperature), cell's voltage and power pulse parameters [81,82]. These are then stored in characteristic maps (CM) in a

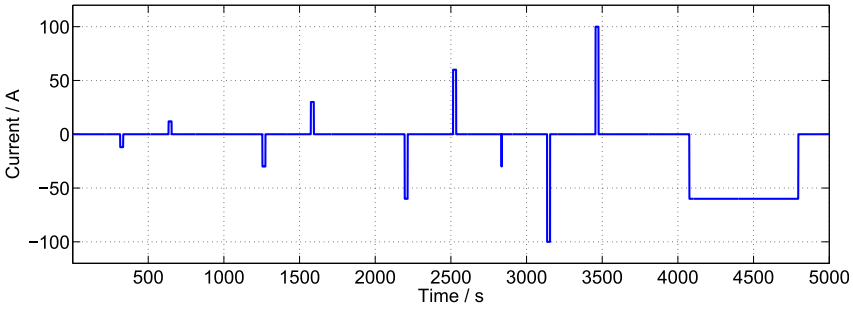

Fig. 6. Current cycle consisting of several pulses.

non-volatile memory of the electronic control unit (ECU). Drawbacks here, CM may be based on synthetic profiles, which are not able to cover all real driving situations leading to static battery characteristics. Furthermore, the adaptation process may adapt infrequent occurrences of extreme load wrongly. The second group of techniques is based on simplified dynamic battery models which extrapolates future cell voltages with higher accuracy [83,84]. These parameter estimations use various versions of the recursive filter estimator. Even though model based prediction is the more reliable method for available power prediction, the current as well as the temperature dependency has not be considered in the literature.

After extensive discussions and a careful evaluation of the principles used in the literature for parameter and state estimation the conclusion is that most of the requirements for on-line battery monitoring algorithms are not met. It is important to consider the limitations of the measurement electronics and available computing power, therefore sophisticated algorithms cannot be complex and high demanding in memory. In addition, BMS has to consider external influences such as temperature variations and different load profiles and has to further adapt its paramterization during the battery lifetime accordingly. Mostly, it has not been taken into account that BMS has to fulfill functional safety in a certain situation or for a particular safety level, therefore, e.g. soft computing algorithms are thus unsuitable.

4. Characterization of the battery impedance for parameter identification algorithm

Before the proposed parameter identification algorithm can be used to determine the states of the battery, the estimated parameters have to be verified.

4.1. Verification by current pulse test

It is possible to determine the overall resistance of the battery by applying a pulse current signal on the battery and evaluating the resulting voltage response. The resulting resistance of the battery can be calculated using Ohms law.

$$R_{\text{ohmic}} = \frac{\Delta V_0}{\Delta I} \tag{1}$$

However, due to the complexity of a battery, following points need to be kept in mind. The instantaneous current pulse results in an immediately voltage drop ΔV_0 over the pure ohmic battery resistance as described in Eq. (1). The second voltage drop ΔV_1 occurs as a result of the charge transfer reaction. Further voltage drop is caused by the change of lithium surface concentration of the active mass particle resulting in a concentration gradient so that diffusion current flows leading to a change in electromotive force (EMF) [4]. In many applications the knowledge of direct-current-resistance (DCR) (Fig. 5).

$$R_{\text{DRC}} = \frac{\Delta V_0 + \Delta V_1}{\Delta I} \tag{2}$$

is considered sufficient, for example when talking about power prediction in EV/HEV with a time frame of about 30 s. However, this simplification does not fully describe the battery dynamics. By way of example, DCR depends on the non-linearity of the charge transfer reaction characterized by Butler–Volmer equation [4]. This would involve that numerous current pulses for charging and discharging (Fig. 6) must be applied on the test bench in the laboratory to extract the current dependency of the battery resistance.

To reduce the influence of the change in EMF and diffusion process, the following successive discharging and charging current pulses are applied, each pulse lasting for 10 s.

4.2. Impedance spectroscopy

Compared to the DCR method, the impedance spectroscopy provides further information about the dynamic behavior of the battery. During impedance spectroscopy (EIS) the battery is excited with small sinusoidal currents of different frequency. The voltage response is recorded and the complex impedance for each excitation frequency can be calculated using the Fourier transformation. The result is the frequency spectrum of the battery around a certain working point. This can be plotted either in a Nyquist diagram or in a Bode plot. Using a sinusoidal current for excitation in impedance spectroscopy is known as the galvanostatic approach. A superimposed DC-current allows to adjust the working point of the battery. It would be possible to use a sinusoidal voltage source for excitation instead, known as the potentiostatic approach and record the current response. However this approach could change the state of charge of the battery since it cannot be assured that the same current that flew in the battery during the positive half-wave is also being taking out during the negative voltage half-wave [85]. Therefore the galvanostatic approach is used.

Since batteries show a strong non-linear behavior, the differential impedance is especially for low frequencies not equal to the quotient of voltage drop under load and current [86]. At low frequencies the sinusoidal excitation can take several minutes. The measurement changes the state of charge and thus the working point of the battery. The requirement of linear time-invariance, which is required for impedance spectroscopy, is violated. To allow quasi-linear measurements, the battery is only excited with small signals around a working point. This prevents a significant change of the state of charge. As mentioned before the working point can be adjusted by a DC-current I_{DC}. Measurements at several

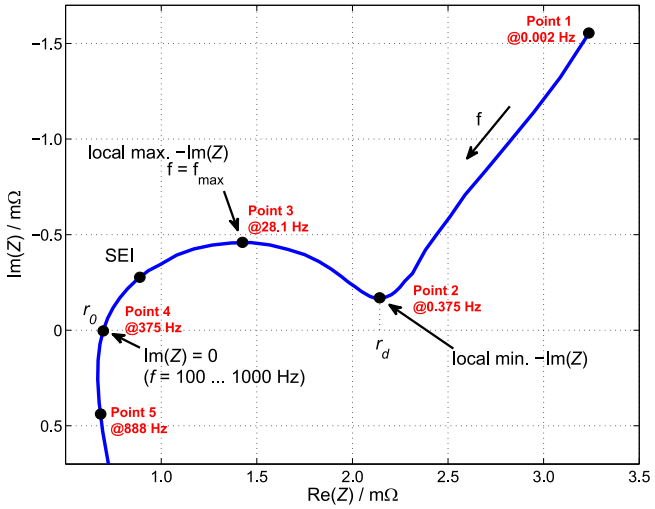

Fig. 7. Nyquist plot of the complex impedance of a Kokam 40 Ah lithium-ion battery with NMC cathode at 10 °C and 90% SOC.

working points are conducted and integrated to obtain a nonlinear characteristic of the battery [87].

$$\underline{Z} = \frac{\mathrm{d}\underline{U}}{\mathrm{d}\underline{I}} \neq \frac{\underline{U}}{\underline{I}} \tag{3}$$

$$U = \int Z(I_{\mathrm{DC}})\mathrm{d}I_{\mathrm{DC}} \tag{4}$$

The complex impedance visible in the Nyquist plot of a battery depends on the state of charge, temperature, health of the battery and current flowing in or out of the battery [86]. An exemplary result in form of an Nyquist plot of a lithium-ion battery (cell K-1) can be found in Fig. 7.

The Nyquist plot of the Kokam 40 Ah cell shows an offset along the real impedance axis. At very high frequencies above ≈800 Hz the spectrum shows an inductive behavior because it follows along the imaginary axis to $\mathrm{Im}(Z) \overset{(\omega)\to\infty}{\longrightarrow} \infty$. At about $\mathrm{Re}(Z) \approx 0.6\ \mathrm{m\Omega}$ the impedance spectrum crosses the real axis. For lower frequencies the impedance spectrum shows a capacitive semicircle which reaches its maximum at $\mathrm{Re}(Z) \approx 1.4\ \mathrm{m\Omega}$, $\mathrm{Im}(Z) \approx -0.5\ \mathrm{m\Omega}$. For very low frequencies in the range of mHz and less the impedance spectrum increases in a capacitive manner in both real- and imaginary part. The characteristic points in Fig. 7 describe the battery dynamics as following:

- The point 4 at $\mathrm{Im}(Z) = 0$ can only be in the wide possible sense compared to the pure ohmic resistance r_0 from Eq. (1) due to the fact that different methods of measurement are applied. This follows from the fact that for EIS the battery shows for different frequencies capacitive and inductive behavior. At a certain frequency where $\mathrm{Im}(Z) = 0$ capacitive and inductive behavior are balanced and only the pure ohmic with additional resistances remains [4].
- Point 2 r_{d} can be broadly defined as the DCR from Eq. (2). At the high frequencies of the semi-circle between r_{d} and r_0 the solid-electrolyte interface (SEI) is indicated and evolves a second smaller semi-circle during aging. The general semi-circle represents the charge transfer reaction in combination with the double layer capacitance. For the investigated cells the SEI semi-circle is comparatively small for new condition and therefore negligible. The corresponding charge-transfer resistance is approximated by

$$r_{\mathrm{ct}} = r_{\mathrm{d}} - r_0 \tag{5}$$

- At point 3 the frequency reaches the local maximum and determines the battery dynamic for voltage response after current change. During aging, the radius of the semi-circle increases and therefore the local maximum then wanders towards lower frequencies, meaning the time constant becomes higher and the voltage response is slower for current changes [4].
- Point 3 illustrates the starting frequency for this EIS measurement.
- At point 5 for high frequencies (starting from positive imaginary part of the impedance spectrum) the effect of inductance is visible and its impedance increases with frequency. Due to the fact that battery packs are often assembled with long wires between the actual electrodes or cell types are formed into compact cylinders leading to leakage inductances which are generally higher than battery impedances.

4.3. Open circuit behavior

The terminal voltage U_{ter} is calculated from four components:

$$U_{\mathrm{ter}} = U_{\mathrm{OCV}} + U_{\mathrm{ohmic}} + U_{\mathrm{react}} + U_{\mathrm{diff}} \tag{6}$$

The open-circuit voltage (OCV) results from the active materials used at the two electrodes. It is directly proportional to the free enthalpy ΔG of the reaction. The number of electrons n, which are transmitted at a reaction, is constant, as is the Faraday's number F.

$$U_{\mathrm{OCV}} = \frac{\Delta G}{n \cdot F} \tag{7}$$

Since the free enthalpy is strongly dependent on concentration effects, the open circuit voltage varies with changing state of charge and temperature. The dependency on the previous history results in the so called OCV hysteresis, where a pronounced difference between the OCV after charge and discharge remains.

The reaction voltage U_{react} describes the change in the open circuit voltage dependent of current across the boundary layers of the two electrodes. The Butler–Volmer equation provides a mathematical description in Eq. (8).

U_{Diff} describes changes in the voltage based on the concentration gradient. This occurs when a battery is charged or discharged with a high current for a long time. Like any diffusion process this is highly dependent on the temperature.

5. Modeling of the battery

The beforehand mentioned states (state of charge (SoC), state of health (SoH), state of function (SoF)) of a battery cannot be directly measured from the battery. Instead a battery model needs to be employed. The battery model is fed with the measurement data. These are the current flowing in or out of the battery, the terminal voltage and temperature measurements inside the battery pack. The parameters of the battery model can be determined by the voltage response of the battery. From the battery model states of the battery can be extracted which are not directly measurable at the actual battery. Therefore, in this section an equivalent circuit battery model based on the results of impedance spectroscopy is introduced. The requirements of the model as well as the physical background of each component of the equivalent circuit model is discussed. Furthermore, the model will be simplified in a way that the on-line determination of the parameters of the battery model becomes possible.

5.1. Requirements of a battery-model

The purpose of the model is to deliver state information for a battery pack which is operated in an electric vehicle during conventional driving operations. Therefore, the validity of the battery model can be limited to condition that are encountered in the above mentioned operational environment. The batteries considered in this work are the 40 Ah and 2 Ah nickel–manganese–cobalt-oxide cathode based lithium-ion battery cells. Additionally the battery impedance estimation is also performed on a lithium-iron phosphate cell from o.m.t. GmbH. Their properties are summarized in the second paper. The specifications of the battery cells can be found in the second paper.

It will be assumed that these specification are valid for the entire driving operation. Since during driving of an electric vehicle both charging while regenerative breaking and discharging of the battery cell occurs, the harder limit has to be applied for the temperature range. A normal driving operation last for a maximal duration of two hours. Longer driving periods are not only not recommended by law [88], they are also not possible because costs of electric-vehicle batteries lead to reduced battery capacity which will most likely not change in the near future. Therefore, the dynamic behavior of the battery cell has to be considered down to the frequency of about 15 mHz. A driving profile consists of several sudden breaking and accelerating moments, 2–3 min stopping as well as longer periods of constant current demand for highway driving. A current demand plot for a driving profile that represents all of these situations is applied in the second paper of our work.

The battery state of charge should not reach 0% during driving operation. Although the self-discharge rate of lithium-ion batteries is very low, it still occurs and the battery will be seriously damaged if the minimal open circuit voltage falls below the limit. Furthermore a modern electric vehicle not only needs energy for traction but also for a wide range of other consumers such as on-board controller, safety devices and so on. Therefore, it will be assumed that the battery of an electric vehicle will not be discharged further than to 80% depth of discharge. Another aspect is an increase of impedance in the depth of discharge range of 80%–100% [89]. This will lead to an increase heat production of the battery and a reduction in power capability. The desired model of the battery cell must be able to reproduce the behavior of the battery within the boundaries (SOA). If this is the case, the data from the battery model can be used to extract the immeasurable states of the real battery cell.

5.2. Extended equivalent circuit model

This section starts with developing an extended equivalent circuit model of the battery based on the composition of the battery dynamic effects occurring during operation of the battery. By the mean of impedance spectroscopy this model is simplified so it can be used for online parameter estimation. Several chemical effects occur during battery operation. To receive a suitable model, all of these effects should be considered and modeled. The battery consists of two electrodes, conducting material for example the current collectors and the electrolyte. Conducting material such as the current collectors at the electrodes or wires inside the battery and the limited conductivity of the electrolyte cause an ohmic voltage drop. This voltage drop is part of the polarization. It can be modeled by a serial resistance [90]. Due to metallic connections inside the cell (for example at the poles or the current collectors) an inductive behavior might occur which can be modeled by an inductance [91]. Mainly at the transitions of electrolyte and the electrodes chemical effects occur. All effects together cause complex impedances for each electrode. They are impedance caused by the SEI at the anode, impedance caused by the charge-transfer process and the double-layer at the electrodes and impedance caused by diffusion processes inside the electrodes (Fig. 8).

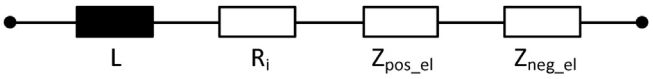

Fig. 8. Equivalent circuit model of a battery cell [91].

6. Simplification of the full order equivalent circuit model

With the results of the impedance spectroscopy, a simplification of the full order equivalent circuit model can be motivated as a basis of battery monitoring algorithms in form of equivalent circuit model (ECM) illustrated in Fig. 9.

It is expected that the effects of the charge-transfer process, the double-layer and the diffusion can be modeled for each electrode. This is not possible because the chemical effects of both electrodes occur at nearly identical time-constants thus they cannot be distinguished in the impedance spectrum. However, this result can be used to simplify the equivalent circuit model for the battery by combining the impedances of both electrodes. Another simplification can be conducted if the necessary frequency range of the model is considered. At very high frequencies of more than 800 Hz the battery shows an inductive behavior. The corresponding time-constant is 1.25 ms. It can be assumed that an excitation with such a high frequency will not occur during normal operation of an electric vehicle. Therefore the inductivity can be neglected [92]. The effect of the SEI on the impedance spectrum is the same as the influence of the charge-transfer process, except it occurs at a higher frequency between the fundamental frequency of the charge-transfer process and the inner resistance. For a high power lithium-ion battery the influence of the SEI is so small that it is not visible in the impedance spectrum. Thus it can be neglected in the equivalent circuit model. However this is only possible as long as no second semicircle becomes visible in the impedance spectrum. For several types of batteries films formed at the electrodes or at one of the electrodes have to be considered [93]. Aging also affects the growth of the SEI and thus the influence of the SEI on the impedance might become significant [5]. The semicircle in the impedance spectrum caused by the charge-transfer process and the double-layer can be modeled by a ZARC-element. A ZARC-element consists of several RC-circuit with slightly different time-constants. Each RC-circuit causes a symmetric semicircle in the impedance spectrum. If the overlapping semicircles are very close to each other, it is possible to simplify the ZARC-element to one single RC-circuit [90,93].

6.1. Double-layer capacitance

The capacitive behavior is caused by a double layer that is formed due to the charges (ions and electrons) that are separated at the boarder of the electrodes towards the liquid electrolyte [94]. The capacitance is a function of the voltage at the double-layer [90].

6.2. Charge-transfer resistance

In parallel a resistance models the charge-transfer process that occurs during intercalation. The charge-transfer process can be described by the Butler–Volmer equation which gives a current–voltage relation with which the resistance can be determined [89].

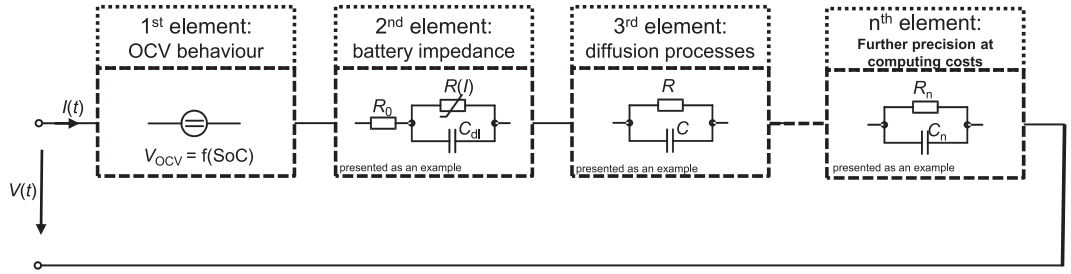

Fig. 9. General form of the ECM of lithium-ion battery [4].

$$I_r = A \cdot i_0 \cdot \left(\exp\left(\frac{\alpha_a \cdot F}{R_{gas} \cdot T} \cdot \Delta U_r \right) - \exp\left(-\frac{\alpha_c \cdot F}{R_{gas} \cdot T} \cdot \Delta U_r \right) \right) \quad (8)$$

$$R(I_r) = \frac{U_r}{I_r} \quad (9)$$

The two exponential terms represent the redox reaction occurring at the electrodes under equilibrium condition. The parameter A models the active surface which changes during aging. The parameter i_0 describes the exchange-current-density which depends on the stiffness of the reaction. If i_0 is high, the voltage only changes slightly with increasing current. These indicates that the value for the charge-transfer resistance depends nonlinearly on the current. The parameter T is the temperature, R_{gas} stands for the universal gas-constant and F for the Faraday-constant. The values of α_a and α_c depend on the symmetry of the reaction between charging and discharging [89].

6.3. Diffusion

To model the diffusion which becomes obvious in the Nyquist diagram at very low frequency a Warburg impedance is added to the Faradaic branch of the RC-circuit [90]. An exact explanation of the Warburg impedance follows in Section 6.4.1. So far the Warburg impedance can be seen as another capacitive circuit. Because the time constant of the diffusion is by more than one order of magnitude different from the time constant of the charge-transfer and double-layer process, it can be removed from the Faradaic branch of the RC-circuit and added in series to the rest of the circuit [90,91]. The simplified equivalent circuit model with the corresponding effects in the Nyquist diagram is shown in Fig. 10.

6.4. Modeling the influence of diffusion

The mass transport inside the battery occurs due to the effect of diffusion. Concentration gradients drive the movement of the ions inside the solid electrodes and the liquid electrolyte. The diffusion can be described by Fick's law, where N_i is the flux of material i in mol s^{-2} cm^2, D_i denotes the material specific diffusion coefficient in cm^2 s^{-1}, c_i describes the concentration of material i in mol cm^{-3} and z describes the direction of transport in cm [95].

$$N_i = -D_i \cdot \frac{dc_i}{dz} \quad (10)$$

According to Jossen [95] the temperature plays a significant role in how fast the diffusion process occurs inside the battery cell. Furthermore, the current demand can be limited by the diffusion process because lithium-ions might not diffuse fast enough to the place of charge-transfer due to limited diffusion [91]. Therefore, an over-potential is caused by reduced or increased ion concentration at the location of the charge-transfer [95]. It is difficult to model the diffusion process precisely with a series of linear elements. Therefore in this section some approximations are employed to develop a diffusion model with linear electric circuit elements. A method for the identification of the parameters of the diffusion model is introduced as well as a methodology to adjust the parameters for different temperatures.

6.4.1. The Warburg element

The Warburg element represents the diffusion process occurring inside the electrodes and the electrolytes. It represents the impedance term in electrochemistry that describes the diffusion process [91]. According to Barsourkov [96], Buller, Jossen et al. [91,95] the Warburg element may represent one out of three possible diffusion

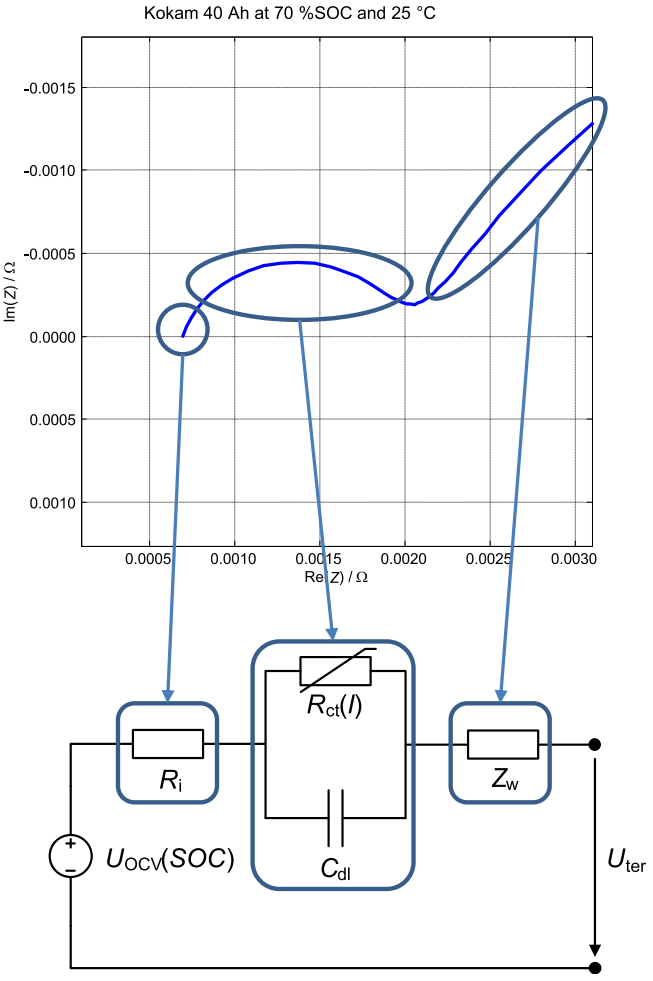

Fig. 10. Simplified equivalent circuit model.

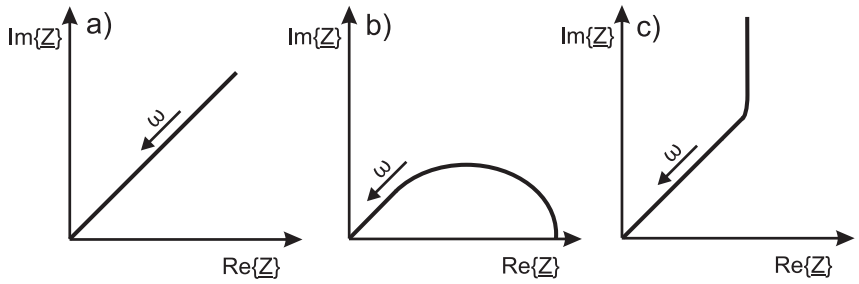

Fig. 11. Complex impedance caused by diffusion processes with a) quasi-infinite diffusion-length, b) limited diffusion length but unlimited reservoir and c) limited diffusion length with non-permeable wall as boundary [95].

types which differ in the assumed boundary conditions. The diffusion process is visible in the Nyquist-plot of the complex impedance of the battery at low frequencies. Depending on the complex impedance one out of the three boundary conditions for the diffusion describing Warburg impedance can be chosen. All three boundary condition for the diffusion process cause an impedance spectrum that follows a slope of $\varphi = -45°$ for high enough frequencies. This behavior can be described by a complex impedance.

$$Z_w = \frac{RT}{cn^2F^2A_e}\cdot\frac{1}{\sqrt{j\omega D}}, \tag{11}$$

The constant R represents the universal gas constant, T stands for temperature, c represents the molarity, n the charge number, F is the Faraday constant, A_e represents the active surface area and D stands for the material depending diffusion coefficient. At lower frequencies the impedance behavior changes depending on the boundary condition (Fig. 11).

- *Quasi-infinite diffusion-length* causing impedance spectra a) at low frequencies

$$Z_w = \frac{RT}{cn^2F^2A_e}\cdot\frac{1}{\sqrt{j\omega D}}, \tag{12}$$

- *Limited diffusion length with unlimited reservoir* causing impedance spectra b) at low frequencies

$$Z_w = \frac{RT}{cn^2F^2A_e}\cdot\frac{\tanh\left(l\cdot\sqrt{j\omega/D}\right)}{\sqrt{j\omega D}} \tag{13}$$

- *Limited diffusion length with non-permeable wall as boundary* causing impedance spectra c) at low frequencies

$$Z_w = \frac{RT}{cn^2F^2A_e}\cdot\frac{\coth\left(l\cdot\sqrt{j\omega/D}\right)}{\sqrt{j\omega D}} \tag{14}$$

6.4.2. Approximation of the Warburg element by equivalent circuit elements

To be able to simulate the diffusion behavior in real time the complex Warburg impedance must be modeled as a time continuous element. Therefore a transformation from the frequency domain to the time domain has to be found. Since the boundary conditions of limited diffusion length are the most realistic the Warburg impedances (13) and (14) will be used.

According to Buller and Mauracher in Refs. [91] and [90] a diffusion resistance R_d and capacitance C_d can be introduced.

$$R_d = \frac{l\cdot RT}{D\cdot cn^2F^2A_e} \tag{15}$$

$$C_d = \frac{l\cdot cn^2F^2A_e}{RT} \tag{16}$$

By applying Eq. (15) on Eq. (14), the Warburg impedances can be simplified and mapped onto the Laplace-domain using $j\omega\rightarrow s$.

$$Z_{w,b} = \sqrt{\frac{R_d}{sC_d}}\cdot\tanh\left(\sqrt{R_d\cdot sC_d}\right) \tag{17}$$

$$Z_{w,c} = \sqrt{\frac{R_d}{sC_d}}\cdot\coth\left(\sqrt{R_d\cdot sC_d}\right) \tag{18}$$

6.4.3. Approximation of the Warburg element by porous electrode model

Eq. (18) represents an infinite number of serial resistances and capacitances because it is mathematically identical to a porous electrode model developed by de Levie in Refs. [91,97]. For a complete equivalent circuit modeling of the diffusion process an unlimited chain of serial resistances and capacitances would be needed. In a conventional simulation tool/BMS low cost microcontroller this is not feasible. However the behavior of the equivalent circuit in Fig. 12 can be approximated by cutting off the equivalent circuit after a certain number N of chain elements. Increasing the number of RC circuits, will improve the approximation of the ZARC elements at the cost increasing processing performance. This means that a compromise between simulation accuracy and computation effort was found to be 5 RC elements. The overall system can be represented in state space. The voltages of the capacitances $U_{c,i}$ are defined as states, the current I is defined as input and the overall voltage U_d as output.

$$U_d = \{1\ \ 0\ \ 0\ \ \dots\ \ 0\ \ 0\ \ 0\}\cdot\mathbf{U_c} + \cdot\frac{R_d}{N}\cdot I$$

$$\dot{\mathbf{U}}_\mathbf{c} = \frac{N^2}{R_d\cdot C_d}\begin{Bmatrix} -1 & 1 & 0 & \dots & 0 & 0 & 0 \\ 1 & -2 & 1 & \dots & 0 & 0 & 0 \\ \vdots & \vdots & \vdots & \ddots & \vdots & \vdots & \vdots \\ 0 & 0 & 0 & \dots & 1 & -2 & 1 \\ 0 & 0 & 0 & \dots & 0 & 1 & -1 \end{Bmatrix}\cdot\mathbf{U_c} + \frac{N}{C_d}\cdot\begin{Bmatrix} 1 \\ 0 \\ \vdots \\ 0 \\ 0 \end{Bmatrix}\cdot I \tag{19}$$

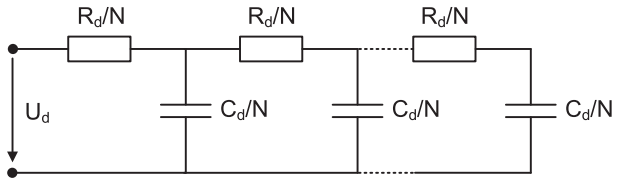

Fig. 12. Equivalent circuit model for the diffusion as proposed in Refs. [91,97].

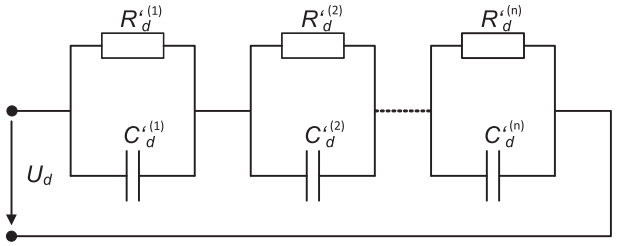

Fig. 13. Equivalent circuit model for the impulse response of the diffusion as proposed in Refs. [90,91].

6.4.4. Approximation of the Warburg element by inverse Laplace-transformation

Another approach to approximate the complex Warburg impedance from Eq. (13) can be found by applying an inverse Laplace transformation on Eq. (17). A Laplace-correspondence table is used to find the impulse response in the time-domain for a given Laplace-domain system. According to Mauracher et al. in Refs. [90,98] provides the following correspondence.

$$\sqrt{\frac{R_d}{sC_d}}\cdot\tanh\left(\sqrt{R_d\cdot sC_d}\right)\ \bullet\!\!-\!\!\circ\ \frac{2}{C_d}\sum_{n=1}^{\infty}\exp\left(\frac{-(2n-1)^2\pi^2}{4\cdot R_dC_d}\cdot t\right) \tag{20}$$

If Eq. (20) is compared with the impulse response of a parallel resistance and capacitance circuit it will become obvious that Eq. (20) can be represented as a chain of parallel RC-elements as illustrated in Fig. 13. The parameters of the equivalent circuit element in Fig. 13 can be found by comparison of the coefficients [90].

$$R_{\mathrm{d}}^{n} = \frac{8\cdot R_{\mathrm{d}}}{(2n-1)^2\pi^2} \tag{21}$$

$$C_{\mathrm{d}}^{n} = \frac{C_{\mathrm{d}}}{2} \tag{22}$$

The new approximation can also be written in state space representation.

$$U_{\mathrm{d}} = \{1\quad 1\quad 1\quad \ldots\quad 1\quad 1\quad 1\}_N\cdot\mathbf{U_c}$$

$$\dot{\mathbf{U}}_{\mathbf{c}} = \frac{1}{R'_{\mathrm{d}}\cdot C'_{\mathrm{d}}}\begin{Bmatrix} -1 & 0 & 0 & \ldots & 0 & 0 & 0\\ 0 & -1 & 0 & \ldots & 0 & 0 & 0\\ \vdots & \vdots & \vdots & \ddots & \vdots & \vdots & \vdots\\ 0 & 0 & 0 & \ldots & 0 & -1 & 0\\ 0 & 0 & 0 & \ldots & 0 & 0 & -1 \end{Bmatrix}\cdot\mathbf{U_c} + \frac{1}{C'_{\mathrm{d}}}\cdot\begin{Bmatrix}1\\1\\\vdots\\1\\1\end{Bmatrix}\cdot I \tag{23}$$

Buller in Ref. [91] explicitly notes that the representations of the Warburg element in Eqs. (19) and (23) base on the impulse response of the underlying frequency representation Eq. (14) and Eq. (13). Therefore the chain of RC-circuits is only valid for linear systems. Using it on a nonlinear system such as a battery system might introduce errors. Therefore in the upcoming parts of this work, referring to the second paper, both approximations for the Warburg element are used and compared to each other in order to evaluate, which approximation produces better results.

7. Parameter identification technique

In order to be able to evaluate the states of the battery, the parameters of the model need to be determined. It can be pointed out that batteries for electric vehicles are built as battery packs each containing up to several hundreds (20…200) of individual battery cells. Since the battery cell with the highest impedance limits the power capability of an entire battery pack, the impedance characteristic for each cell needs to be determined [32]. With the impedance information and the open circuit voltage information of each cell the state of charge, state of health and power capability of the entire battery pack can be determined. It is necessary to determine the model parameters online because the instantaneous power capability of the battery packs depends on the parameters of each battery cell and the parameters change in a highly nonlinear current depending manner which is very difficult to predict offline, especially if each individual cell needs to be considered. Another reason for online determination is that failure of the battery pack can only be predicted if the parameters of each cell are known at every moment in time.

Because of the huge number of battery cells within a battery pack, a fast and memory saving algorithm needs to be developed. This allows the implementation into a battery management system which monitors hundreds of battery cells.

The discrete time representation is necessary to allow the implementation on embedded system hardware. A discrete time parameter estimator is employed to determine the parameters of the inner resistance, the charge-transfer process and the double-layer capacitance. These parameters are remapped onto the time continuous domain for evaluation purposes and state determination. Until that point a piecewise linear dependency between measured voltage and current is assumed. To correct the assumption of piecewise linear dependency, the nonlinear dependency of the parameter describing the charge-transfer process due to the redox reaction occurring at the electrodes is considered by a nonlinear current depending parameter correction algorithm based on the Butler–Volmer equation. A diffusion model will describe the influence of the diffusion on the overall impedance of the battery cell.

7.1. Identification of the dynamics of the battery

The equivalent circuit model developed in Section 6 contains a lumped network of three elements and the diffusion impedance which is a distributed element. The identification of the three lumped network elements is discussed in this section.

7.1.1. Discrete time parameter mapping

To allow the supervision of the battery states at each moment of operation and to consider the nonlinear character of the parameters, the parameter identification must be performed online. Although the battery state of health does not change with high dynamics, the battery state of charge and especially the state of function can change during operation. Because the supervising system such as the battery management system works on a digital processing unit, the signal processing is performed in discrete time steps. Also the current, voltage and temperature sensors will provide information only at discrete points of time. Therefore a transformation of the battery model proposed in Section 6 from the time continuous domain to a discrete time domain must be performed.

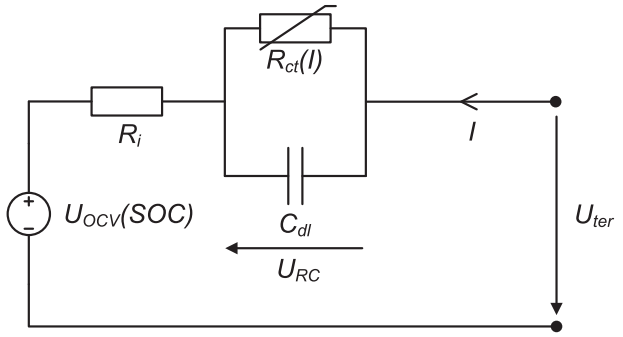

Fig. 14. Equivalent circuit model without diffusion for online parameter estimation.

Furthermore the diffusion process is separated from the charge-transfer process because the time constants of both processes are far apart [86]. This allows a separate determination of the parameters. Without the diffusion impedance for the diffusion process the equivalent circuit can be reduced to a first order system with a voltage source, a series resistance and a first order RC-element. The new circuit is shown in Fig. 14. The unknown parameters of this circuit in the time continuous domain can be described by a vector θ. The aim of the online parameter estimation technique is to determine these parameters in dependency of the input signal for later use in the state determination process.

$$\theta = \begin{pmatrix} R_i \\ R_{\mathrm{ct},0} \\ C_{\mathrm{dl}} \\ e \end{pmatrix} \tag{24}$$

with $R_{\mathrm{ct},0}$ as charge-transfer resistance with assumed linear current dependency. The voltage U_{RRC} will solely depend on the first three parameters of the parameter-vector θ. The parameter e will contain the open circuit voltage and the diffusion voltage drop.

$$U_{\mathrm{RRC}}(t,\theta) = R_i \cdot I(t) + U_{\mathrm{RC}}(t,\theta) \tag{25}$$

With the help of Kirchhoff's law a time-continuous formulation of the system can be determined.

$$\begin{aligned} U_{\mathrm{RRC}}(t) &= R_i \cdot I(t) + R_{\mathrm{ct},0} \cdot I_{\mathrm{r}}(t) \\ \Leftrightarrow U_{\mathrm{RRC}}(t) &= R_{\mathrm{ct},0} \cdot \left(I(t) - C_{\mathrm{dl}} \cdot \frac{\mathrm{d}U_{\mathrm{RC}}(t)}{\mathrm{d}t} \right) + R_i \cdot I(t) \\ \Leftrightarrow U_{\mathrm{RRC}}(t) &= \left(R_i + R_{\mathrm{ct},0}\right) \cdot I(t) + \left(R_i R_{\mathrm{ct},0} C_{\mathrm{dl}}\right) \cdot \frac{\mathrm{d}I(t)}{\mathrm{d}t} \\ &\quad - \left(R_{\mathrm{ct},0} C_{\mathrm{dl}}\right) \cdot \frac{\mathrm{d}U_{\mathrm{RRC}}(t)}{\mathrm{d}t} \end{aligned} \tag{26}$$

It is obvious that continuous time differentiation is necessary to describe the dynamic behavior of the equivalent circuit model. Therefore we perform a time discretization of the system equation by mapping Eq. (26) into the z-domain. For that the system is described in the Laplace domain which is possible because the system is causal. A forward Euler approach is used for the transformation from the Laplace-domain to the z-domain.

$$\begin{aligned} U_{\mathrm{RRC}}(t) &= \left(R_i + R_{\mathrm{ct},0}\right) \cdot I(t) + \left(R_i R_{\mathrm{ct},0} C_{\mathrm{dl}}\right) \cdot \frac{\mathrm{d}I(t)}{\mathrm{d}t} \\ &\quad - \left(R_{\mathrm{ct},0} C_{\mathrm{dl}}\right) \cdot \frac{\mathrm{d}U_{\mathrm{RRC}}(t)}{\mathrm{d}t} \end{aligned}$$

$$\begin{aligned} \circ\!\!-\!\!\bullet \quad U_{RRC}(s) &= I(s) \cdot (R_i + R_{ct,0}) + \\ &\quad s \cdot I(s) \cdot (R_i R_{ct,0} C_{dl}) - \\ &\quad s \cdot U_{RRC}(s) \cdot (R_{ct,0} C_{dl}) \end{aligned} \tag{27}$$

The forward Euler approach uses a difference equation to approximate the differentiation. The difference equation uses a stepsize T_{s} which determines the sampling frequency. Higher order transformation would increase the precession at the cost of calculation time.

$$s \;\circ\!\!-\!\!\bullet\; \frac{1 - z^{-1}}{T_s z^{-1}} \tag{28}$$

$$\begin{aligned} U_{\mathrm{RRC}}\left(z^{-1}\right) &= I\left(z^{-1}\right) \cdot \left(R_i + R_{\mathrm{ct}}\right) + \frac{1 - z^{-1}}{T_{\mathrm{s}} z^{-1}} \cdot I\left(z^{-1}\right) \cdot \left(R_i R_{\mathrm{ct}} C_{\mathrm{dl}}\right) \\ &\quad - \frac{1 - z^{-1}}{T_{\mathrm{s}} z^{-1}} \cdot U_{\mathrm{RRC}}\left(z^{-1}\right) \cdot \left(R_{\mathrm{ct}} C_{\mathrm{dl}}\right) \end{aligned}$$

Algebraic transformations are necessary to be able to see the discrete time form of the overall system function (26). The aim is to have the term z^{-1} standing alone in front of the current $I(z^{-1})$ and the voltage $U_{\mathrm{RRC}}(z^{-1})$.

$$U_{\mathrm{RRC}}\left(z^{-1}\right) = I\left(z^{-1}\right) \cdot \underbrace{R_i}_{b_0} + z^{-1} \cdot I\left(z^{-1}\right) \cdot \underbrace{\left(\frac{T_{\mathrm{s}}}{C_{\mathrm{dl}}} + \frac{T_{\mathrm{s}} R_i}{C_{\mathrm{dl}} R_{\mathrm{ct}}} - R_i\right)}_{b_1} - z^{-1} \cdot U_{\mathrm{RRC}}\left(z^{-1}\right) \cdot \underbrace{\left(\frac{T_{\mathrm{s}}}{C_{\mathrm{dl}} R_{\mathrm{ct}}} + 1\right)}_{a_1} \tag{29}$$

The term z^{-1} in the z-domain stands for a sample-and-hold unit in the discrete time domain. It becomes obvious that instead of having to differentiate the signal it is now possible to simple hold the previous signal for one time step T_{s}. This makes the integration into a discrete running digital system possible. The variable k denotes the current discrete time-step.

$$z^{-1} \;\bullet\!\!-\!\!\circ\; \delta(k-1) \tag{30}$$

After performing the inverse z-transformation using (29) and (30), a time-discrete formulation of the system described in (26) is achieved.

$$U_{\mathrm{RRC}}(k) = b_0 \cdot I(k) + b_1 \cdot I(k-1) - a_1 \cdot U_{\mathrm{RRC}}(k-1) \tag{31}$$

A new parameter vector θ_{d} for the discrete system equation has been introduced.

$$\theta_{\mathrm{d}} = \begin{pmatrix} b_0 \\ b_1 \\ a_1 \\ e \end{pmatrix} \tag{32}$$

The discrete parameter set can be described by the continuous parameter set θ. To allow remapping from the discrete time domain

to the time continuous domain, the discrete parameters vector θ_d needs to be mapped on the continuous time parameter vector θ.

$$\begin{aligned} b_0 &= R_i \quad R_i = b_0 \\ b_1 &= \frac{T_s}{C} + \frac{T_s R_i}{C_{dl} R_{ct}} - R_i \quad R_{ct} = \frac{b_1 - b_0 a_1}{a_1 + 1} \\ a_1 &= \frac{T_s}{C_{dl} R_{ct}} + 1 \quad C_{dl} = \frac{T_s}{b_1 - b_0 a_1} \end{aligned} \tag{33}$$

7.1.2. Reformulation to acknowledge time varying characteristics

Setting the voltage $U_{ter}(k)$ from Fig. 14 as the output-signal $y(k)$ of the system and the current $I(k)$ as the input-signal $u(k)$ of the system, Eq. (31) describes an ARX-model. AR refers to the auto-regressive part described by the parameter a_1 and the output $y(k)$ and X refers to the input described by the parameters b_0, b_1 and the input $u(k)$ [99]. Furthermore the parameter e is added as an extra voltage which is not described by U_{RRC}. A battery cell's impedance characteristic strongly depends on temperature, aging, state of charge and current demand. While aging and temperature are external parameters that are not supposed to change with fast dynamics and the state of charge also does not change rapidly, the current demand might change with high dynamics. Therefore it cannot be assumed that it is enough to estimate one single set of parameters θ for the entire driving cycle. The parameter-set θ changes over the estimation time and therefore has to be estimated continuously. Because the parameters do not change instantaneously it is not necessary to estimate the parameters at each single time step k. This leads to a piecewise linear formulation of the overall system. For small time steps T_s it is assumed that the battery cell behaves as a linear system. However looking at the overall picture a battery cell does not show linear characteristics since its behavior strongly depends on external influences. That is why the linear model needs to be re-estimated often enough [31]. Nonlinear characteristics of the charge transfer process will be assumed linear for the parameter regression approach. At a later step this assumption will be corrected by a nonlinear parameter identification technique described in the second part. Denoting the parameter-vector as time-depending $\theta(k)$, introducing a regression vector $\varphi(k)$ and recognizing the influence of the e-parameter leads to reformulation of Eq. (31).

$$\varphi(k) = \begin{pmatrix} u(k) \\ u(k-1) \\ y(k) \\ 1 \end{pmatrix} \tag{34}$$

$$\hat{y}(k, \theta_d(k)) = \varphi^T(k)\theta_d(k) \tag{35}$$

The term $\hat{y}(k, \theta_d(k))$ denotes the voltage estimated by a given parameter-set $\theta_d(k)$ and a given regression vector $\varphi(k)$.

In order to estimate the parameters and states, we will use the derived state-space model of the battery. In the second paper a novel state of charge determination algorithm has been developed which bases on the residual term of the least-square parameter identification algorithm. Because the parameters of the battery model are updated online, the state of health can be tracked by observing the change of resistance. Especially the increase of the charge-transfer resistance reflects the aging process. To evaluate the state of function, the power capability of the battery is analyzed by evaluating the identified resistances of the battery model.

8. Conclusion

In this paper we have described the algorithmic requirements of monitoring algorithms of the BMS in EV/HEV applications. After a careful review of commonly used monitoring algorithms, it became clear that the majority of the proposed methods is not suitable as a basis for real-time-capable BMS. The reason for this lies in the fact that no particular attention is paid to the limitations of low-cost target microcontroller in cases where complex and computationally high demanding mathematical algorithms are proposed and applied to simple linear dependency battery models. Therefore, this first paper eliminates certain weak points addressed in the literature review by designing a novel simplified battery model in state-space structure. The battery model has been extended by incorporating a current depending charge transfer resistance. A Warburg element represents the mass transport effects occurring during operation of the lithium-ion battery.

In the second paper we will employ a weighted recursive least quadratic square parameter estimator which allows an efficient online identification of the high dynamic elements of the developed battery model. The identification algorithm is fully recursive and can be easily implemented on an embedded system.

References

[1] D. Linden, T.B. Reddy, Handbook of Batteries, third ed., McGraw-Hill, New York, 2002.
[2] M. Becker, G. Traufetter, Boeing Wählte Brandgefährliches Batteriematerial, 21.03.2013. Der Spiegel Online, URL: http://www.spiegel.de/wissenschaft/technik/dreamliner-akkus-boeing-waehlte-brandgefaehrliches-batteriematerial-a-878759.html.
[3] K. Reif, Bosch Autoelektrik und Autoelektronik, Bosch Fachinformation Automobil, Vieweg + Teubner, 2011. URL: http://books.google.de/books?id=8N9caMHk7IUC.
[4] W. Waag, Adaptive Algorithms for Monitoring of Lithium-ion Batteries in Electric Vehicles (Ph.D. thesis), RWTH Aachen University, 2013. submitted to department of electrical engineering.
[5] W. Waag, S. Käbitz, D.U. Sauer, Appl. Energy 102 (0) (2013) 885–897.
[6] W. Waag, C. Fleischer, D.U. Sauer, J. Power Sources 258 (0) (2014) 321–339.
[7] S. Buller, in: 2nd, International Advanced Automotive Battery Conference, 202.
[8] V.S.-M.R. Mingant, J. Bernard, in: 26th Electric Vehicle Symposium 2012, Los Angeles, USA, 2002.
[9] G.L. Plett, J. Power Sources 134 (2) (2004) 277–292, http://dx.doi.org/10.1016/j.jpowsour.2004.02.033.
[10] M. Wahlstrom, Design of a Battery State Estimator Using a Dual Extended Kalman Filter (Ph.D. thesis), University of Waterloo, 2010.
[11] G.L. Plett, J. Power Sources 161 (2) (2006) 1356–1368, http://dx.doi.org/10.1016/j.jpowsour.2006.06.003.
[12] G.L. Plett, J. Power Sources 161 (2) (2006) 1369–1384, http://dx.doi.org/10.1016/j.jpowsour.2006.06.004.
[13] R. van der Merwe, Sigma-point Kalman Filters for Probabilistic Inference in Dynamic State-space Models (Ph.D. thesis), OGI School of Science & Engineering, Oregon Health & Science University, Portland, OR, USA, April 2004.
[14] G. Plett, in: 21st Electric Vehicle Symposium (EVS21), 2005.
[15] C. Hu, B.D. Youn, J. Chung, Appl. Energy 92 (C) (2012) 694–704. URL: http://EconPapers.repec.org/RePEc:eee:appene:v:92:y:2012:i:c:p:694-704.
[16] J. Kim, S. Lee, B.H. Cho, IEEE Trans. Power Electron. 27 (1) (2012) 436–451, http://dx.doi.org/10.1109/TPEL.2011.2158554.
[17] G. Plett, State and Parameter Estimation for an Electrochemical Cell, no. 8103485 (B2), 2012. URL: http://patent.ipexl.com/US/08103485.html.
[18] D. Haifeng, W. Xuezhe, S. Zechang, in: Vehicle Power and Propulsion Conference, 2009, VPPC '09, IEEE, 2009, pp. 1649–1653. URL: http://dx.doi.org/10.1109/VPPC.2009.5289654.
[19] H. Dai, X. Wei, Z. Sun, J. Wang, W. Gu, Appl. Energy 95 (0) (2012) 227–237, http://dx.doi.org/10.1016/j.apenergy.2012.02.044. URL: http://www.sciencedirect.com/science/article/pii/S0306261912001432.
[20] D.V. Do, C. Forgez, K. El-Kadri-Benkara, G. Friedrich, IEEE Trans. Veh. Technol. 58 (8) (2009) 3930–3937, http://dx.doi.org/10.1109/TVT.2009.2028572.
[21] R. Xiong, F. Sun, Z. Chen, H. He, Appl. Energy 113 (2014) 463–476.
[22] G. Plett, System and Method for Determining Both an Estimated Battery State Vector and Battery Parameter Vector, no. 7521895 (B2), 2009. URL: https://www.google.com/patents/US7521895.
[23] F. Zhang, G. Liu, L. Fang, in: ICRA '09. IEEE International Conference on Robotics and Automation, 2009, 2009, pp. 1863–1868, http://dx.doi.org/10.1109/ROBOT.2009.5152745.

[24] M. Samadi, S. Alavi, M. Saif, in: American Control Conference (ACC), 2013, 2013, pp. 4693–4698.
[25] M. Verbrugge, D. Frisch, B. Koch, J. Electrochem. Soc. 152 (2) (2005) A333–A342, http://dx.doi.org/10.1149/1.1847658 arXiv: http://jes.ecsdl.org/content/152/2/A333.full.pdf+html. URL: http://jes.ecsdl.org/content/152/2/A333.abstract.
[26] M. Verbrugge, B. Koch, J. Electrochem. Soc. 153 (1) (2006) A187–A201, http://dx.doi.org/10.1149/1.2128096 arXiv: http://jes.ecsdl.org/content/153/1/A187.full.pdf+html. URL: http://jes.ecsdl.org/content/153/1/A187.abstract.
[27] M. Verbrugge, J. Appl. Electrochem. 37 (5) (2007) 605–616, http://dx.doi.org/10.1007/s10800-007-9291-7. URL: http://www.ingentaconnect.com/content/klu/jach/2007/00000037/00000005/00009291.
[28] L. Juang, P. Kollmeyer, T. Jahns, R. Lorenz, in: Energy Conversion Congress and Exposition (ECCE), 2010, IEEE, 2010, pp. 3903–3910, http://dx.doi.org/10.1109/ECCE.2010.5617776.
[29] X.-S. Hu, F.-C. Sun, Y. Zou, J. Cent. South Univ. Technol. (2011) 1525–1531, http://dx.doi.org/10.1007/s11771-011-0869-1.
[30] J. Lee, Y. Kim, H. Cha, in: Energy Conversion Congress and Exposition (ECCE), 2011, IEEE, 2011, pp. 1489–1494, http://dx.doi.org/10.1109/ECCE.2011.6063957.
[31] S. Wang, M. Verbrugge, J.S. Wang, P. Liu, J. Power Sources 196 (20) (2011) 8735–8741, http://dx.doi.org/10.1016/j.jpowsour.2011.06.078. URL: http://www.sciencedirect.com/science/article/pii/S0378775311013152.
[32] M. Roscher, O. Bohlen, D. Sauer, IEEE Trans. Energy Convers. 26 (3) (2011) 737–743, http://dx.doi.org/10.1109/TEC.2011.2155657.
[33] L. Mandal, R. Cox, in: Energy Conversion Congress and Exposition (ECCE), 2011, IEEE, 2011, pp. 2635–2640, http://dx.doi.org/10.1109/ECCE.2011.6064121.
[34] J. Sabatier, M. Aoun, A. Oustaloup, G. Grgoire, F. Ragot, P. Roy, Signal Process. 86 (10) (2006) 2645–2657, http://dx.doi.org/10.1016/j.sigpro.2006.02.030. Special Section: Fractional Calculus Applications in Signals and Systems, URL: http://www.sciencedirect.com/science/article/pii/S0165168406000533.
[35] K. Smith, C. Rahn, C.-Y. Wang, in: IEEE International Conference on Control Applications, 2008, CCA 2008, 2008, pp. 714–719, http://dx.doi.org/10.1109/CCA.2008.4629589.
[36] K. Smith, C. Rahn, C.-Y. Wang, IEEE Trans. Control Syst. Technol. 18 (3) (2010) 654–663, http://dx.doi.org/10.1109/TCST.2009.2027023.
[37] A.P. Schmidt, M. Bitzer, Árpád W. Imre, L. Guzzella, J. Power Sources 195 (22) (2010) 7634–7638, http://dx.doi.org/10.1016/j.jpowsour.2010.06.011. URL: http://www.sciencedirect.com/science/article/pii/S0378775310009948.
[38] S. Moura, N. Chaturvedi, M. Krstic, in: American Control Conference (ACC), 2012, 2012, pp. 559–565.
[39] S. Moura, N. Chaturvedi, M. Krstic, in: American Control Conference (ACC), 2012, 2012, pp. 566–571.
[40] M.K. Scott, J. Moura, N.A. Chaturvedi, in: Proceedings of the 2012 ASME Dynamic Systems and Control Conference, 2012, pp. 101–110, http://dx.doi.org/10.1115/DSCC2012-MOVIC2012-8800.
[41] A.P. Schmidt, M. Bitzer, Árpád W. Imre, L. Guzzella, J. Power Sources 195 (15) (2010) 5071–5080, http://dx.doi.org/10.1016/j.jpowsour.2010.02.029. URL: http://www.sciencedirect.com/science/article/pii/S0378775310002740.
[42] N. Chaturvedi, R. Klein, J. Christensen, J. Ahmed, A. Kojic, IEEE Control Syst. Mag. 30 (3) (2010) 49–68, http://dx.doi.org/10.1109/mcs.2010.936293.
[43] R. Klein, N. Chaturvedi, J. Christensen, J. Ahmed, R. Findeisen, A. Kojic, in: American Control Conference (ACC), 2010, 2010, pp. 6618–6623.
[44] R. Klein, N. Chaturvedi, J. Christensen, J. Ahmed, R. Findeisen, A. Kojic, IEEE Trans. Control Syst. Technol. 21 (2) (2013) 289–301, http://dx.doi.org/10.1109/TCST.2011.2178604.
[45] J.V. Michael, A. Roscher, Oliver Bohlen, Int. J. Electrochem. 2011 (1) (2011) 69–84.
[46] M.A. Roscher, Zustandserkennung von $LiFePO_4$-Batterien fr Hybrid- und Elektrofahrzeuge (Ph.D. thesis), RWTH Aachen University, 2010.
[47] M.A. Roscher, D.U. Sauer, J. Power Sources 196 (1) (2011) 331–336, http://dx.doi.org/10.1016/j.jpowsour.2010.06.098. URL: http://www.sciencedirect.com/science/article/pii/S0378775310010852.
[48] X. Tang, X. Zhang, B. Koch, D. Frisch, in: International Conference on Prognostics and Health Management, 2008, PHM 2008, 2008, pp. 1–12, http://dx.doi.org/10.1109/PHM.2008.4711432.
[49] X. Tang, X. Zhang, Y.-K. Chin, B.J. Koch, D.R. Frisch, Model-based Estimation of Battery Hysteresis, US 7957921 B2, (2011).
[50] H.S. Steven Hoening, Thirumalai G. Palanisamy, Method for Determining State of Charge of a Battery by Measuring its Open Circuit Voltage, 2002.
[51] Y. Yang, J. Liu, C. Tsai, J. Chin. Inst. Eng. 31 (2) (2008) 313–322, http://dx.doi.org/10.1080/02533839.2008.9671384 arXiv: http://www.tandfonline.com/doi/pdf/10.1080/02533839.2008.9671384. URL: http://www.tandfonline.com/doi/abs/10.1080/02533839.2008.9671384.
[52] V. Pop, H. Bergveld, D. Danilov, P. Regtien, P. Notten, Battery Management Systems: Accurate State-of-Charge Indication for Battery-Powered Applications, Philips Research Book Series 9, Springer Verlag, London, 2008. URL: http://doc.utwente.nl/64893/.
[53] J. Li, J.K. Barillas, C. Guenther, M.A. Danzer, J. Power Sources 230 (0) (2013) 244–250, http://dx.doi.org/10.1016/j.jpowsour.2012.12.057. URL: http://www.sciencedirect.com/science/article/pii/S0378775312019039.
[54] S. Yuan, H. Wu, C. Yin, Energies 6 (1) (2013) 444–470, http://dx.doi.org/10.3390/en6010444. URL: http://www.mdpi.com/1996-1073/6/1/444.
[55] C. Zhang, J. Jiang, W. Zhang, S.M. Sharkh, Energies 5 (4) (2012) 1098–1115, http://dx.doi.org/10.3390/en5041098. URL: http://www.mdpi.com/1996-1073/5/4/1098.
[56] A. Rahmoun, H. Biechl, A. Rosin, in: Electric Power Quality and Supply Reliability Conference (PQ), 2012, 2012, pp. 1–4, http://dx.doi.org/10.1109/PQ.2012.6256238.
[57] J. Uhlmann, Dynamic Map Building and Localization: New Theoretical Foundations, University of Oxford, 1995. URL: http://books.google.com/books?id=eJb4MgEACAAJ.
[58] S. Julier, J. Uhlmann, H. Durrant-Whyte, IEEE Trans. Autom. Cont. 45 (3) (2000) 477–482, http://dx.doi.org/10.1109/9.847726.
[59] S. Julier, J. Uhlmann, Proc. IEEE 92 (3) (2004) 401–422, http://dx.doi.org/10.1109/JPROC.2003.823141.
[60] E.A. Wan, R.V.D. Merwe, in: Kalman Filtering and Neural Networks, Wiley, 2001, pp. 221–280.
[61] Z. He, M. Gao, C. Wang, L. Wang, Y. Liu, Energies 6 (8) (2013) 4134–4151, http://dx.doi.org/10.3390/en6084134. URL: http://www.mdpi.com/1996-1073/6/8/4134.
[62] L. Wang, L. Wang, C. Liao, J. Liu, in: Vehicle Power and Propulsion Conference, 2009, VPPC '09, IEEE, 2009, pp. 1592–1595, http://dx.doi.org/10.1109/VPPC.2009.5289604.
[63] H. Dai, X. Wei, Z. Sun, Przegld Elektrotechniczny R. 88 (1b) (2012) 57–63.
[64] K.G. Matthew Daigle, in: Annual Conference of the Prognostics and Health Management Society, 2010, pp. 1–12.
[65] H. Dai, X. Wei, Z. Sun, in: Proceedings of the 2009 International Conference on Measuring Technology and Mechatronics Automation – Volume 02, ICMTMA '09, IEEE Computer Society, Washington, DC, USA, 2009, pp. 375–380, http://dx.doi.org/10.1109/ICMTMA.2009.333.
[66] F. Sun, X. Hu, Y. Zou, S. Li, Energy 36 (5) (2011) 3531–3540, http://dx.doi.org/10.1016/j.energy.2011.03.059. URL: http://www.sciencedirect.com/science/article/pii/S0360544211002271.
[67] J. Yan, G. Xu, Y. Xu, B. Xie, in: ICARCV, 2008, pp. 464–469.
[68] M. Orchard, P. Hevia-Koch, B. Zhang, L. Tang, IEEE Trans. Ind. Electron. 60 (11) (2013) 5260–5269, http://dx.doi.org/10.1109/TIE.2012.2224079.
[69] F. Zhang, G. Liu, L. Fang, in: 7th World Congress on Intelligent Control and Automation, 2008, WCICA 2008, 2008, pp. 989–994, http://dx.doi.org/10.1109/WCICA.2008.4593055.
[70] S. Santhanagopalan, R.E. White, Int. J. Energy Res. 34 (2) (2010) 152–163, http://dx.doi.org/10.1002/er. 1655.
[71] A. Cuadras, O. Kanoun, in: 6th International Multi-Conference on Systems, Signals and Devices, 2009, SSD '09, 2009, pp. 1–5, http://dx.doi.org/10.1109/SSD.2009.4956761.
[72] Z. Chen, S. Qiu, M. Masrur, Y. Murphey, in: The 2011 International Joint Conference on Neural Networks (IJCNN), 2011, pp. 2156–2163, http://dx.doi.org/10.1109/IJCNN.2011.6033495.
[73] M. Charkhgard, M. Farrokhi, IEEE Trans. Ind. Electron. 57 (12) (2010) 4178–4187, http://dx.doi.org/10.1109/TIE.2010.2043035.
[74] C. Cai, D. Du, Z. Liu, in: The 12th IEEE International Conference on Fuzzy Systems, 2003, FUZZ '03, vol. 2, 2003, pp. 1068–1073, http://dx.doi.org/10.1109/FUZZ.2003.1206580.
[75] T. Wu, M. Wang, Q. Xiao, X. Wang, Smart Grid Renew. Energy 3 (2012) 51–55.
[76] M. Einhorn, F. Conte, C. Kral, J. Fleig, in: 2010 IEEE International Conference on Sustainable Energy Technologies (ICSET), 2010, pp. 1–6, http://dx.doi.org/10.1109/ICSET.2010.5684928.
[77] K.S.D. Ha, I. Cho, in: Proceedings of the 26th International Battery, Hybrid and Fuel Cell Electric Vehicle Symposium (EVS26), 2012 http://dx.doi.org/10.1109/ICSET.2010.5684928.
[78] M. Roscher, J. Assfalg, O. Bohlen, IEEE Trans. Veh. Technol. 60 (1) (2011) 98–103, http://dx.doi.org/10.1109/TVT.2010.2090370.
[79] S. Lee, J. Kim, J. Lee, B.H. Cho, in: Power Electronics Specialists Conference, 2007, PESC 2007, IEEE, 2007, pp. 2799–2803, http://dx.doi.org/10.1109/PESC.2007.4342462.
[80] R. Hwu, B.Y. Liaw, M. Dubarry, V. Svoboda, Electrochem. Solid-State Lett (2006).
[81] Dirk Uwe Sauer, P. Birke, M. Keller, Oliver Bohlen, Jochen Gerschler, in: 22nd Electric Vehicle Symposium (EVS22), Yokohama, Japan, 2006.
[82] J.W. Andre Boehm, Adaptives verfahren zur bestimmung der maximal abgebaren oder aufnehmbaren leistung einer batterie, WO 2011095368 A1, 2011.
[83] F. Sun, R. Xiong, H. He, W. Li, J.E.E. Aussems, Appl. Energy 96 (0) (2012) 378–386, http://dx.doi.org/10.1016/j.apenergy.2012.02.061. Smart Grids, URL: http://www.sciencedirect.com/science/article/pii/S0306261912001626.
[84] L. Juang, P. Kollmeyer, T. Jahns, R. Lorenz, in: Energy Conversion Congress and Exposition (ECCE), 2012, IEEE, 2012, pp. 1819–1826, http://dx.doi.org/10.1109/ECCE.2012.6342591.
[85] G. Pilatowicz, in: Anleitungen zum Batteriepraktikum, Institut für Stromrichtertechnik und elektrische Antriebe, Aachen, 2013.
[86] S. Buller, M. Thele, R. De Doncker, E. Karden, IEEE Trans. Ind. Appl. 41 (3) (2005) 742–747.
[87] J. Kowal, Spatially-resolved Impedance of Nonlinear Inhomogeneous Devices – Using the Examploe of Lead-acid Batteries (Ph.D. thesis), RWTH Aachen University, 2010.
[88] European Parlament and Council of the EU, Off. J. 102 (2006) 1–14.
[89] D.U. Sauer, in: J. Garche (Ed.), Encyclopedia of Electrochemical Power Sources, Elsevier B.V., Ulm, 2009, pp. 443–451.
[90] P. Mauracher, E. Karden, J. Power Sources 67 (1) (1997) 69–84.
[91] S. Buller, Impedance Based Simulation Models for Energy Storage Devices in Advanced Automotive Power Systems (Ph.D. thesis), RWTH Aachen University, 2003.

[92] V. Pop, H.J. Bergveld, D. Danilov, P. Regtien, P. Notten, Battery Management Systems Accurate State-of-Charge Indication, Vol. 9 of Philips Research Book Series, Springer, Netherlands, Dordrecht, 2008.
[93] A.E. Anders, Effect of Current Dynamics on Li-ion Cell Capacity and Impedance (Ph.D. thesis), University of Wisconsin, Madison, 2010.
[94] H. Helmholtz, Ann. Phys. Chem. 7 (8) (1879) 337–382.
[95] A. Jossen, W. Weydanz, Moderne Akkumulatoren richtig einsetzen, Inge Reichardt Verlag, 2006.
[96] E. Barsoukov, J. Macdonald, Impedance Spectroscopy: Theory, Experiment, and Applications, Wiley, 2005. URL: http://books.google.de/books?id=8hNkOWO/_DLwC.
[97] R.D. Levie, Electrochim. Acta 9 (9) (1964) 1231–1245.
[98] M.R. Spiegel, Schaum's Outline of Theory and Problems of Laplace Transforms, McGraw-Hill, New York, 1965.
[99] L. Ljung, System Identification Theory for the User, second ed., Prentice Hall Inc., Upper Saddle River, 1999.